Programmed assembly of 3-dimensional microtissues with defined cellular connectivity

Zev J. Gartner[a,1] and Carolyn R. Bertozzi[a,b,c,d,2]

Departments of [a]Chemistry and [b]Molecular and Cell Biology, [c]Howard Hughes Medical Institute, University of California, Berkeley, CA 94720; and [d]The Molecular Foundry, Lawrence Berkeley National Laboratory, Berkeley, CA 94720

Contributed by Carolyn R. Bertozzi, January 23, 2009 (sent for review November 26, 2008)

Multicellular organs comprise differentiated cell types with discrete yet interdependent functions. The cells' spatial arrangements and interconnectivities, both critical elements of higher-order function, derive from complex developmental programs in vivo and are often difficult or impossible to emulate in vitro. Here, we report the bottom-up synthesis of microtissues composed of multiple cell types with programmed connectivity. We functionalized cells with short oligonucleotides to impart specific adhesive properties. Hybridization of complementary DNA sequences enabled the assembly of multicellular structures with defined cell–cell contacts. We demonstrated that the kinetic parameters of the assembly process depend on DNA sequence complexity, density, and total cell concentration. Thus, cell assembly can be highly controlled, enabling the design of microtissues with defined cell composition and stoichiometry. We used this strategy to construct a paracrine signaling network in isolated 3-dimensional microtissues.

DNA | self-assembly | bottom-up synthesis | cell-cell signaling

Cells live and communicate within oriented 3-dimensional environments by exchanging electrical, chemical, and contact-dependent signals. The convergence of these signals defines unique microenvironments that have important consequences for a myriad of cellular processes, including control of the cell cycle, migratory potential, and differentiation state. Contact-dependent signals between cells, in particular, are determinants of the short-range structure and behavior of tissues. For example, disruption of contact-dependent signals in a 3D in vitro model of human breast acini causes healthy tissue to switch from a normal to a tumor-like phenotype or, conversely, can coerce tumor-derived cells to organize into architectures that behave like healthy tissue (1). Similarly during development, cell–cell contacts occurring in topologically distinct microenvironments provide cues that induce otherwise identical cells to differentiate along divergent pathways (2, 3). Finally, specific contacts occurring between stem cells and the surrounding stroma are crucial for proper organization and maintenance of adult stem cell niches from diverse tissues and organisms (4).

Reconstituting functional cell–cell contacts ex vivo and in 3 dimensions remains an important challenge in tissue engineering, whether for the purpose of building materials for in vivo tissue repair or for constructing realistic in vitro tissue models. Although considerable progress has been made toward defining the interactions between cells and their surrounding matrix (5), the ability to control interconnectivity among cells in 3 dimensions has been elusive. Bottom-up strategies such as layer-by-layer printing (6), directed assembly using dielectrophoretic forces (7, 8) or lasers (9–12), and a variety of lithographic techniques (13, 14) have produced 2D cellular arrays of multiple cell types (7, 12–14) or defined 3D cell aggregates of a single cell type (8, 15, 16). However, these methods may not be readily applicable to generating multicellular structures with controlled interconnectivity in 3 dimensions.

An alternative bottom-up strategy is exemplified by the approach of synthetic chemists, who typically construct complex molecules by the controlled stepwise formation of bonds between simple building blocks. Likewise, we envisioned a bottom-up approach to the construction of microtissues with defined connectivities by stepwise formation of contacts between individual cells (supporting information (SI) Fig. S1*b*). Such a method requires a means to endow 2 cells with mutual reactivity as well as the ability to purify products (multicellular structures) away from unreacted starting materials (individual cells). We recently reported a method for functionalizing cell surfaces with oligonucleotides for the purpose of cell patterning on complementary DNA-coated surfaces (17). Here, we report that hybridization between DNA-coated cells can direct the assembly of cell–cell contacts as shown schematically in Fig. 1*A*. We used this bonding interaction to build 3D microtissues with defined interconnectivities from the bottom up.

Results and Discussion

Activating Mutual Reactivity Between 2 Populations of Cells. To establish conditions for controlled cell assembly, Jurkat cells were first labeled with cytosolic fluorescein or Texas Red dyes to distinguish them in mixed populations. They were then surface functionalized with complementary ("matched") or noncomplementary ("mismatched") single-stranded DNA (ssDNA) 20-mers by using a procedure similar to that previously described (17). In brief, cultured cells were metabolically labeled with *N*-azidoacetylmannosamine (ManNAz, Fig. S1*d*) and the resulting cell surface azido sialic acid (SiaNAz) residues were reacted by Staudinger ligation (18) with phosphine-conjugated ssDNA or by copper-free click chemistry with difluorinated cyclooctyne (DIFO)-conjugated ssDNA (Fig. S1*c*) (19). When combined in a 1:1 ratio, cells bearing no cell surface DNA (Fig. 1*B*) or mismatched oligonucleotides (Fig. 1*C*) showed no specific interactions. However, cells functionalized with matched DNA underwent polymerization to form large aggregates with little control over the final architecture (Fig. S2*a Right*).

To control the immediate neighbours of a single cell type and synthesize more uniform structures, we combined the cells at various stoichiometries of >1:50. Under these conditions we observed individual cell clusters (Fig. 1*D*) that, under higher magnification, demonstrated a common architecture in which the microenvironment of the limiting cell type was defined by neighbours of the cell type added in excess (Fig. 1*E*). These clusters formed sequence-specifically, in excellent yield (Fig. S2 *b–d*), and without compromising the cell membrane (Fig. S3). We performed a similar experiment to that in Fig. 1*D* but with cells decorated with oligonucleotides that were conjugated to a fluorescent dye. The labeled oligonucleotides were found to cluster at cell–cell interfaces (Fig. 1*F*), confirming the role of

Author contributions: Z.J.G. and C.R.B. designed research; Z.J.G. performed research; Z.J.G. and C.R.B. analyzed data; and Z.J.G. and C.R.B. wrote the paper.

The authors declare no conflict of interest.

[1]Present address: Department of Pharmaceutical Chemistry, University of California, San Francisco, CA 94158.

[2]To whom correspondence should be addressed. E-mail: crb@berkeley.edu.

This article contains supporting information online at www.pnas.org/cgi/content/full/0900717106/DCSupplemental.

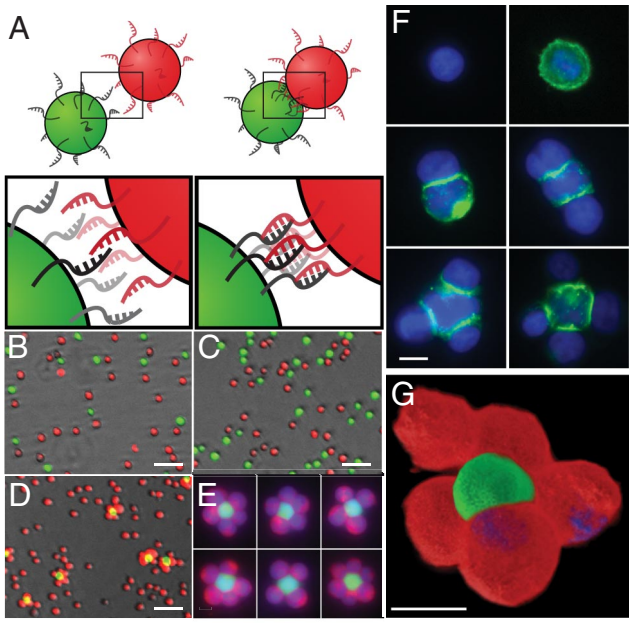

Fig. 1. Oligonucleotides direct the synthesis of 3-dimensional multicellular structures with defined patterns of connectivity. (*A*) Cells bearing complementary cell surface oligonucleotides react to form stable cell–cell contacts. (*B*) Nonadherent Jurkat cells with CMFDA (fluorescein, green) or CMTPX (Texas Red, red) cytosolic stains were combined at a 1:1 ratio. (*C*) Green- and red-stained Jurkat cells labeled with the mismatched oligos 1-Phos and 5′-Phos were also mixed at a 1:1 ratio. (*D*) Green- and red-stained Jurkat cells labeled with the complementary sequences 1-Phos and 1′-Phos and combined at a 1:50 ratio. (*E*) Discrete structures from *D* at higher magnification. (*F*) Cells labeled with fluorescein-conjugated DNA (single cell, *Top Right*) were assembled with cells bearing a nonfluorescent complementary strand (single cell, *Top Left*). (*G*) 3D reconstruction of a single multicellular structure encapsulated in agarose by using deconvolution fluorescence microscopy. Red, Texas Red; green, fluorescein; blue, DAPI. (Scale bars: *B–D*, 50 μm; *E–G*, 10 μm.)

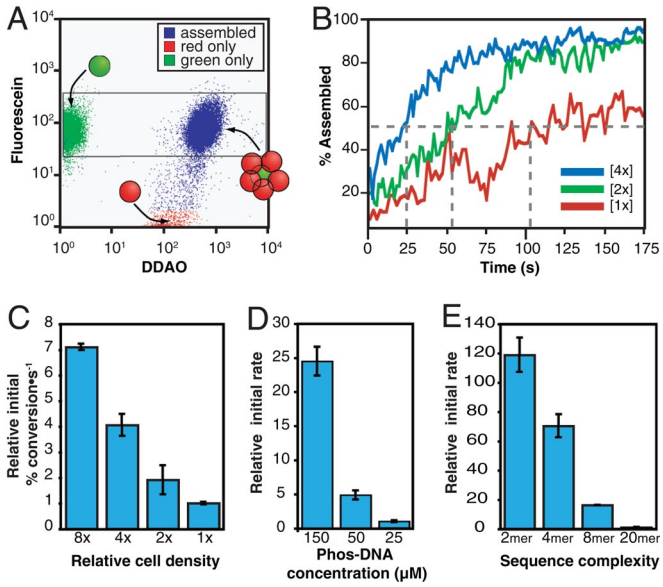

Fig. 2. Kinetic analysis of cell assembly by flow cytometry. (*A*) Green and DDAO-SE (far-red) stained cells were labeled with complementary strands of DNA and mixed at a 1:100 ratio in-line with a flow cytometer. A scatter plot representation of the data showed 3 distinct populations. The conversion of the green population into the blue population was measured as a function of time. (*B*) The resulting kinetic profiles were used to extract information about the assembly process (e.g., 2-fold dilutions of cells in suspension resulted in a corresponding 2-fold decrease in the $t_{1/2}$ of assembly). (*C*) Relative initial rates derived from the data in *B* expressed as initial % conversion·s^{-1}. (*D*) The dependence of initial rates on the density of DNA on the cell surface. The concentration of phosphine-conjugated DNA (Phos-DNA) used in the labeling reactions correlated with cell surface DNA density (Table S1). (*E*) Relative initial rates of green and far-red stained cells labeled with 20-mer DNA comprising the underlying 2-mer, 4-mer, or 8-mer repeats, or a heterogeneous 20-mer sequence. All sequences had identical GC:AT ratios and no predicted stable secondary structures. Cells were labeled with uniform concentrations of their respective Phos-DNA sequences and measurements were performed by using identical cell densities.

DNA duplex formation in directing the synthesis of these structures. Finally, the 3-dimensionality of the structures was confirmed by capturing them in an agarose matrix before imaging by deconvolution fluorescence microscopy (Fig. 1*G*).

Characterizing and Controlling the Kinetics of Microtissue Assembly. With the goal of defining the kinetic and thermodynamic parameters governing the assembly reaction, we analyzed the rate of cell–cell contact formation under a variety of reaction conditions. Appropriately labeled cells were mixed together in line with a flow cytometer at a 1:100 ratio, and the fluorescence properties of the assembling structures were determined in real time (Fig. 2*A*). We observed predictable kinetic properties analogous to molecules reacting in solution. For example, 2-fold dilutions of cells in suspension resulted in a 2-fold decrease in the $t_{1/2}$ for the assembly reaction, an observation consistent with second-order kinetics (Fig. 2 *B* and *C*). We also demonstrated that the rate of assembly depends on the density of the cell surface DNA, a parameter that is dictated by the concentration of phosphine-DNA used in the labeling reaction (Fig. 2*D*). Measurable rates of assembly were observed by using cells with surface DNA densities that varied over nearly 2 orders of magnitude ($\approx$125 to >7,100 oligos per μm^2, Table S1).

We also explored the dependence of the kinetics of cell assembly on oligonucleotide sequence. We synthesized four 20-mer oligonucleotides together with their complementary strands. All pairs shared nearly identical calculated free energies of association (20) but differed in the complexity of the underlying nucleotide sequences. These sequences included a simple CA (and TG) 2-mer repeat, a CCAA (and TTGG) 4-mer repeat, an 8-mer repeat, and a fully heterogeneous 20-mer sequence (see *SI Text*). We observed decreasing rates of assembly as oligonucleotide sequences were made more heterogeneous. As measured by flow cytometry, the initial rate of assembly of these 4 sequences differed by >2 orders of magnitude (Fig. 2*E*), suggesting that the rate-limiting step for assembly highly depends on the number of trajectories available for oligonucleotide annealing (21). Combined, these experiments demonstrate at least 3 independent variables that control reactivity between cells during the assembly process: cell density, cell surface DNA density, and oligonucleotide sequence complexity. Rational manipulation of these variables allows direct control over the size distribution and stoichiometry of assembled products (Fig. S4).

Purification of Assembled Microtissues and Iterative Synthesis. A key feature of our approach is the ability to purify desired multicellular structures away from undesired by-products and individual "unreacted" cells by fluorescence-activated cell sorting (FACS) (Fig. 3*A*). We synthesized multicellular structures comprising red- and green-labeled Jurkat cells and sorted the products with the desired fluorescence properties (Fig. 3*B*). The purified structures retained their cell stoichiometries and topologies as assessed by fluorescence microscopy (Fig. 3*C*). In addition, the integrity of their cell membranes was maintained as assessed by ethidium homodimer exclusion (Fig. S5). We further elaborated the purified cell clusters into larger and more complex structures

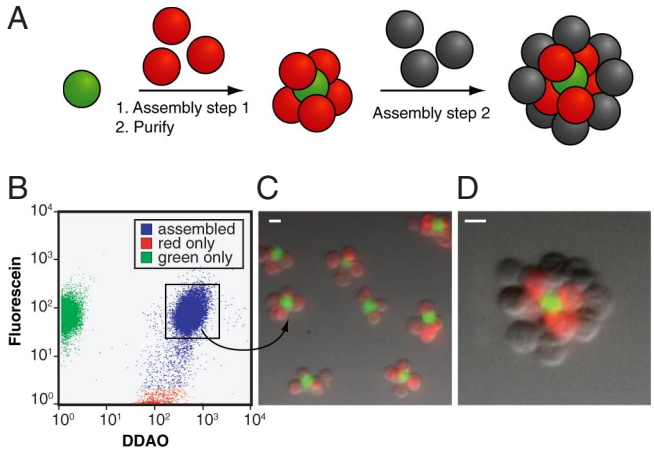

Fig. 3. Fluorescence-activated cell-sorting (FACS) separates cell assemblies based on their fluorescence properties. (*A*) Schematic diagram of multistep assembly of cellular building blocks. (*B*) Jurkat cell-based structures were isolated by FACS based on red and green fluorescence proportional to the number of each cell type in the cluster. (*C*) Fluorescence micrograph of the isolated structures. (*D*) Higher-order multicellular structure generated by incubation of the structures in *C* with a third population of unstained Jurkat cells bearing cell surface oligonucleotides complementary to those on the red-stained cells. Red, Texas Red; green, fluorescein. (Scale bars: 10 μm.)

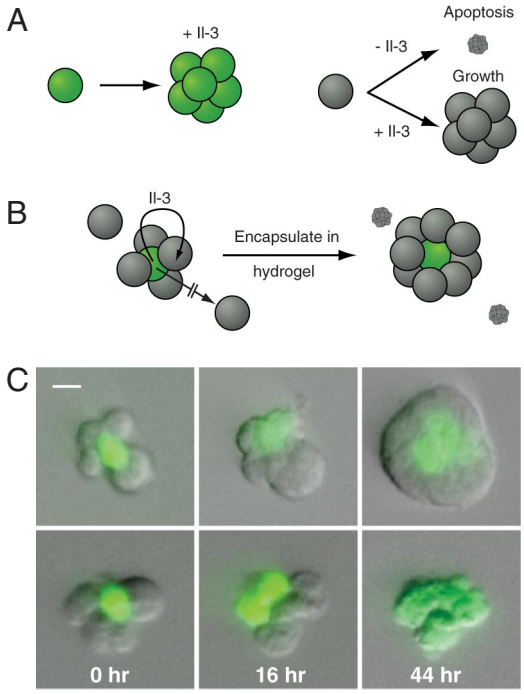

Fig. 4. Construction of a microtissue possessing a paracrine signaling network. (*A*) CHO cells expressing murine IL-3 (and GFP) proliferate independently of external growth factors (green). The murine pro-B cell line FL5.12 undergoes apoptosis in the absence of IL-3 but propagates rapidly in its presence (gray). (*B*) Schematic diagram of 3D tissue construction by programmed assembly of CHO (IL-3) and FL5.12 cells. (*C*) Multicellular structures of different sizes (Fig. S7 and Fig. S8) were synthesized, encapsulated in agarose along with an anti-IL-3 antibody, and their growth monitored by fluorescence microscopy. *Upper* and Fig. S7, structures containing CHO (IL-3). *Lower* and Fig. S8, structures comprising CHO cells that lack IL-3. Green, GFP; gray, DIC. (Scale bar: 10 μm.)

by incubation with a third population of Jurkat cells decorated with the same DNA oligomer as the central fluorescein-labeled cell (Fig. 3*D*). These experiments demonstrate the feasibility of synthesizing microtissues by the iterative stepwise formation of contacts between individual cells.

DNA-Mediated Intercellular Contacts Are Reversible. An advantage of duplex DNA as a bonding agent for cell–cell contacts is the potential for controlled melting or degradation to reverse the linkage. This feature allows for elimination of DNA from cell–cell junctions after microtissue synthesis, provided the structures are stabilized by encapsulation in a solid matrix or by infiltration of the junctions with native adhesion molecules. We investigated 2 strategies to reverse DNA-bound cellular assemblies. First, we used oligonucleotides with a 10-base region of complementarity that form duplexes at 20–25 °C but melt at 37 °C. Cell–cell junctions formed by using these oligonucleotides were stable at room temperature (Fig. S6*a*) but dissociated at 37 °C (Fig. S6*b*). Second, we used DNase to rapidly degrade DNA duplexes (Figs. S6 *c* and *d*). By using either of these 2 approaches, assembled structures could be templated, encapsulated within a suitable 3-dimensional matrix, and the cell surface duplexes removed without disrupting the topology of microtissues.

Synthesizing a Functional Paracrine Signaling Network in 3 Dimensions. The ultimate goal of our approach is the synthesis of microtissues with emergent functional properties that depend on those of the underlying cellular building blocks, as in living tissues. Toward this end, we constructed a system comprising functionally distinct cell types wherein one produces a signal that is critical for the other's growth and survival. The first building block was a CHO cell line engineered to express the secreted growth factor interleukin-3 (IL-3) and the green fluorescent protein (GFP) as a cytosolic reporter. The second was an untransformed hematopoietic progenitor cell line (FL5.12) whose survival and replication depends on the presence of IL-3 (Fig. 4*A*) (22). Withdrawal of IL-3 from FL5.12 cells results in cell cycle arrest and the onset of apoptosis within 12 to 36 h (23).

We synthesized structures of various compositions by using these 2 cell types and the products were embedded within an inert 3-dimensional agarose matrix (Fig. 4*B*). The matrix was also impregnated with an anti-IL-3 antibody to prevent long-range diffusion of the cytokine. The growth of each structure was monitored by fluorescence microscopy. Immediately after implantation and before the first cell division (16 h) little change in morphology was observed (Fig. 4*C Upper* and Fig. S7). However, after 16 h, the structures underwent accelerated growth as IL-3 accumulated in the vicinity of the growing microtissues. In control structures comprising CHO cells lacking the gene encoding IL-3, the FL5.12 cells showed no growth and instead underwent a change in morphology between 16 and 44 h that was consistent with apoptosis (24). By 44 h, the FL5.12 cells had been absorbed by the CHO cells, which had expanded to fill the void left within the agarose matrix (Fig. 4*C Lower* and Fig. S8). Similarly, FL5.12 cells not assembled into structures but encapsulated randomly in the agarose matrix together with IL-3-secreting CHO cells did not grow during the course of the experiment. This simple paracrine signaling network emulates cytokine-dependent immune cell expansion (25, 26) as well as tumor cell proliferation at sites of inflammation (27).

Conclusion

In summary, we assembled 3D microtissues by building connectivities among cells by using duplex DNA as a bonding agent. The process can be performed under typical cell culture conditions, does not require genetic manipulation, and the multicellular products are portable to any environment for fundamental studies or tissue engineering. Duplex DNA is a highly versatile

cellular bonding agent, because oligonucleotide sequences can be readily designed to direct multiple orthogonal cell–cell contacts while avoiding activation of an innate immune response by Toll-like receptors (e.g., exclusion of the sequence CpG) (28). We anticipate this unprecedented control over cellular topology will provide a means of analyzing cellular behavior in vitro as a function of overall tissue architecture. This method may also provide access to fundamental units of tissue function such as the stem cell niche, building blocks for artificial organs and high-throughput screening platforms, and in vitro models of human disease in which multiple cell types collude.

Materials and Methods

Oligonucleotide Sequences

1: 5′-ACTGACTGACTGACTG-3′-C_7 NH_2
1′: 5′-CAGTCAGTCAGTCAGTCAGT-3′-C_7-NH_2
1′-FAM: FAM-5′-CAGTCAGTCAGTCAGTCAGT-3′-C_7-NH_2
2: NH_2-C_6-5′-CACACACACACACACACACA-3′
2′: NH_2-C_6-5′-TGTGTGTGTGTGTGTGTGTG-3′
3: NH_2-C_6-5′-CCAACCAACCAACCAACCAA-3′
3′: NH_2-C_6-5′-TTGGTTGGTTGGTTGGTTGG-3′
4: NH_2-C_6-5′-CCTACATCCCTACATCCCTA-3′
4′: NH_2-C_6-5′-TAGGGATGTAGGGATGTAGG-3′
5: NH_2-C_6-5′-GTAACGATCCAGCTGTCACT-3′
5′: NH_2-C_6-5′-AGTGACAGCTGGATCGTTAC-3′
6: 5′-ACTGACTGACTTTTTTTTTT-3′-C_7-NH_2
6′: 5′-GTCAGTCAGTTTTTTTTTT-3′-C_7-NH_2

General Materials and Methods. Fluoresence and brightfield microscopy images were collected on a Zeiss 200M inverted microscope equipped with an automated sample stage and a temperature-controlled incubator. Image analysis was performed by using SlideBook v4.2 software (Intelligent Imaging). The brightness and contrast of images were adjusted linearly using Slidebook or Adobe Photoshop software in a manner that maintained consistency across a given experiment and its controls.

General Cell Culture Conditions. Jurkat, Chinese Hamster ovary (CHO) and FL5.12 cells were maintained in a 5% CO_2, water-saturated atmosphere at 37 °C with the indicated medium supplemented with 10% fetal bovine serum (FBS, HyClone), penicillin (100 units/mL, Invitrogen), and streptomycin (0.1 mg/mL, Invitrogen) unless otherwise specified. Jurkat cells were grown in RPMI 1640 medium (Gibco), CHO cells in F-12 (HAM) (GIBCO), and FL5.12 cells in RPMI-1640 supplemented with 50 μM β-mercaptoethanol (Sigma) and 3.5 ng/mL murine recombinant IL-3 (Sigma). Cell densities were maintained between 2×10^5 and 2×10^6 cells per mL. The murine IL-3 gene was stably introduced to CHO cells by retroviral infection followed by selection for clones resistant to puromycin at 5–10 μg/mL (29). Secretion of active IL-3 from selected clones was confirmed by the ability of the CHO (IL-3)-conditioned media to support the growth of FL5.12 cells. The gene encoding green fluorescent protein (GFP) was inserted into the vector pCDNA 3.1 and stably introduced to IL-3 secreting CHO cells by transient transfection followed by selection for stable clones with geneticin.

Metabolic Labeling. Solutions of 25 μM (Jurkat), 35 μM (FL5.12), or 50 μM (CHO) Ac_4ManNAz in the appropriate culture media were inoculated with 2×10^5 cells per mL and grown for 3 days.

Cell Surface Labeling. Washed cells were resuspended in purified Phos- or DIFO-conjugated oligonucleotides dissolved in PBS and supplemented with FBS to a final concentration of 1%. Staudinger ligations using Phos-DNA were allowed to proceed for 30 min at 37 °C, whereas reactions with DIFO-DNA were allowed to proceed for 15 min at 37 °C unless indicated otherwise. Cells were pelleted by centrifugation, washed 3 times with reaction buffer, and counted before assembly.

Imaging of Fluorescently Labeled Cell Surface Oligonucleotides. Metabolically labeled cells were washed 3 times in reaction buffer, resuspended in either 125 μM **1**-Phos or 250 μM **1′**-FAM-Phos (Fig. S9), and incubated at 37 °C for 1 h. DNA-labeled cells were washed 3 times to remove unreacted oligonucleotide and the 2 populations of cells were combined at a 1:50 ratio in reaction buffer and shaken at 125 rpm for 45 min at 25 °C. Reactions were quenched by the addition of 1 volume of 50% formaline (Fisher). Aliquots were mixed 1:1 with VECTASHIELD mounting medium containing DAPI (Vector Labs) and analyzed by fluorescence microscopy.

Analysis of Cell Assembly Kinetics by Flow Cytometry. Flow cytometry analysis was performed on a BD FACSCalibur flow cytometer equipped with a 488-nm argon laser and a 635-nm red diode laser. Data were analyzed by using FlowJo software.

Dependence on Cell Densities. Green and far-red stained populations of Jurkat cells were labeled with 100 μM solutions of **1**- and **1′**-Phos, respectively. Green cells were added to silanized (Sigmacote, Sigma-Aldrich) 5-mL polystyrene culture tubes. Assembly reactions were initiated by adding a 100-fold excess of far-red-labeled cells to a final density of 5,000,000 cells per mL (8×). Tubes were quickly placed on the flow cytometer (≈2- to 4-s delay) and agitated by left–right displacement at a rate of one per second. Twofold dilutions resulted in final densities of far-red cells of 2,500,000 (4×), 1,225,000 (2×), and 612,500 cells per mL (1×). Measurements were performed in triplicate and the mean initial rate reported as percent assembled per second (v_0/[green cells]$_0$).

Dependence on Concentration of DNA Used for Cell Labeling. Green- and far-red-stained populations of Jurkat cells were reacted with solutions of **1** or **1′**-Phos, respectively, at concentrations of 25, 100, and 150 μM. Green cells (10,000 cells per mL final density) were added to silanized culture tubes, then far-red cells in reaction buffer (1,000,000 cells per mL final density) were added to start assembly. Reactions were agitated once per second and monitored by flow cytometry. Measurements were performed in duplicate and the mean initial rate was reported as percent assembled per second (v_0/[green cells]$_0$).

Dependence on DNA Sequence Complexity. Green-stained cells were labeled with a 100 μM solution of **2**-Phos, **3**-Phos, **4**-Phos, or **5**-Phos. Far-red-stained cells were labeled with 100 μM solutions of **2′**-Phos, **3′**-Phos, **4′**-Phos, or **5′**-Phos. Cells were collected by centrifugation and washed 3 times with reaction buffer to remove unreacted oligonucleotide. Rates of assembly were measured after adding 10,000 green cells in reaction buffer to silanized 5-mL polystyrene culture tubes, and initiating assembly with the addition of far-red cells to a final density of 1,000,000 cells per mL (a green:far-red ratio of 1:100). Tubes were agitated once per second. Measurements were performed in triplicate, and the mean initial rate reported as percent assembled per second (v_0/[green cells]$_0$).

Synthesis of Multistep Microtissues. Green, red, and unstained populations of metabolically labeled Jurkat cells were washed and reacted with a 100 μM solution of **1**-DIFO (green), a 50 μM solution of **1′**-DIFO (red), or a 50 μM solution of **1**-DIFO (unstained) for 40 min at 37 °C. Populations were washed 3 times in reaction buffer and green and red cells were assembled for 20 min at room temperature, with agitation, at a 1:100 ratio, and by using a total cell density of ≈1,000,000 cells per mL. The assembly reaction was loaded onto a DAKO Cytomations MoFlo high-speed cell sorter (University of California Berkeley Cancer Research Laboratory Flow Cytometry Facility) running at 15 psi and equipped with a 120-μm flow cell tip. Events exhibiting green fluorescence consistent with a single green cell and red fluorescence consistent with 4–6 red cells were selected for sorting. Cell clusters were sorted into one well of a 6-well tissue culture plate containing ≈1,000,000 of the unstained cells labeled with **1**-DIFO, then agitated to facilitate assembly. The assembly reaction was allowed to settle without agitation for 5 min. Three-quarters of the supernatant was removed, replaced with fresh reaction buffer, and images of the assembled products were collected by DIC and fluorescence microscopy.

Generation of a Microtissue Comprising a 3D Paracrine Signaling Network. Metabolically labeled CHO (stably expressing GFP alone, or GFP and murine IL-3) and FL5.12 cells were reacted with **1**- and **1′**-DIFO (100 μM), respectively, for 30 min at 37 °C. FL5.12 cells were washed once with IL-3-containing media. CHO and FL5.12 cells were then washed 3 times with reaction buffer and assembled at a CHO/FL5.12 ratio of 1:60 at high (≈1,500,000 cells per mL) or low (≈150,000 cells per mL) density at 25 °C and with agitation at 125 rpm on an orbital shaker. Aliquots of the assembly reactions were combined with an anti-IL-3 antibody (0.5 μg/mL, Sigma) and type IX ultra-low gelling agarose (Sigma, 0.7% final concentration). A thin layer of this mixture was deposited in 6-well plates and the gel was set by brief chilling at 4 °C. The gel was then overlaid with fresh media (RPMI medium 1640) and the cells allowed to recover for 30 min at 37 °C and 5% CO_2 before imaging. Image collection at the indicated time points proceeded for ≈2 h and included between 20 and 30 observations under each condition (IL-3 (+) vs. IL-3 (−) CHO cells; high density

vs. low density assembly; 2 antibody concentrations (only one shown); CHO cells only; FL5.12 cells only.

ACKNOWLEDGMENTS. We thank Ameeta Kelekar for providing the FL5.12 cell line, Matthew Hangauer, Jeremy Baskin and Julius Codelli for reagents, and Nicholas Treuheit and Hector Nolla for technical assistance. This work was supported by the Nanoscale Science, Energy, and Technology Program of the Department of Energy. Z.J.G. is a fellow of the Jane Coffin Childs Memorial Fund for Medical Research. This investigation has been aided by a grant from the Jane Coffin Childs Memorial Fund for Medical Research.

1. Nelson CM, Bissell MJ (2006) Of extracellular matrix, scaffolds, and signaling: Tissue architecture regulates development, homeostasis, and cancer *Annu Rev Cell Dev Biol* 22:287–309.
2. Yamashita YM, Fuller MT, Jones DL (2005) Signaling in stem cell niches: Lessons from the Drosophila germline. *J Cell Sci* 118:665–672.
3. Priess J. Notch signaling in the *C. elegans* embryo (June 25, 2005), *WormBook*, ed. The *C. elegans* Research Community, WormBook, doi/10.1895/wormbook.1.4.1, http://www.wormbook.org.
4. Li L, Xie T (2005) Stem cell niche: structure and function. *Annu Rev Cell Dev Biol* 21:605–631.
5. Lutolf MP, Hubbell JA (2005) Synthetic biomaterials as instructive extracellular microenvironments for morphogenesis in tissue engineering. *Nat Biotechnol* 23:47–55.
6. Ringeisen BR, Othon CM, Barron JA, Young D, Spargo BJ (2006) Jet-based methods to print living cells. *Biotechnol J* 1:930–948.
7. Chiou PY, Ohta AT, Wu MC (2005) Massively parallel manipulation of single cells and microparticles using optical images. *Nature* 436:370–372.
8. Albrecht DR, Underhill GH, Wassermann TB, Sah RL, Bhatia SN (2006) Probing the role of multicellular organization in three-dimensional microenvironments. *Nat Methods* 3:369–375.
9. Odde DJ, Renn MJ (2000) Laser-guided direct writing of living cells. *Biotechnol Bioeng* 67:312–318.
10. Zhang H, Liu KK (2008) Optical tweezers for single cells. *J R Soc Interface* 5:671–690.
11. Barron JA, Krizman DB, Ringeisen BR (2005) Laser printing of single cells: Statistical analysis, cell viability, and stress. *Ann Biomed Eng* 33:121–130.
12. Nahmias Y, Odde DJ (2006) Micropatterning of living cells by laser-guided direct writing: Application to fabrication of hepatic-endothelial sinusoid-like structures. *Nat Protoc* 1:2288–2296.
13. Falconnet D, Csucs G, Grandin HM, Textor M (2006) Surface engineering approaches to micropattern surfaces for cell-based assays. *Biomaterials* 27:3044–3063.
14. Khademhosseini A, Langer R, Borenstein J, Vacanti JP (2006) Microscale technologies for tissue engineering and biology. *Proc Natl Acad Sci USA* 103:2480–2487.
15. Karp JM, et al. (2007) Controlling size, shape and homogeneity of embryoid bodies using poly(ethylene glycol) microwells. *Lab Chip* 7:786–794.
16. Rosenthal A, Macdonald A, Voldman J (2007) Cell patterning chip for controlling the stem cell microenvironment. *Biomaterials* 28:3208–3216.
17. Chandra RA, Douglas ES, Mathies RA, Bertozzi CR, Francis MB (2006) Programmable cell adhesion encoded by DNA hybridization. *Angew Chem Int Ed Engl* 45:896–901.
18. Saxon E, Bertozzi CR (2000) Cell surface engineering by a modified Staudinger reaction. *Science* 287:2007–2010.
19. Codelli JA, Baskin JM, Agard NJ, Bertozzi CR (2008) Second-generation difluorinated cyclooctynes for copper-free click chemistry. *J Am Chem Soc* 130:11486–11493.
20. Kibbe WA (2007) OligoCalc: An online oligonucleotide properties calculator *Nucleic Acids Res* 35:W43–46.
21. Chan YH, Lenz P, Boxer SG (2007) Kinetics of DNA-mediated docking reactions between vesicles tethered to supported lipid bilayers. *Proc Natl Acad Sci USA* 104:18913–18918.
22. McKearn JP, McCubrey J, Fagg B (1985) Enrichment of hematopoietic precursor cells and cloning of multipotential B-lymphocyte precursors. *Proc Natl Acad Sci USA* 82:7414–7418.
23. Nunez G, et al. (1990) Deregulated Bcl-2 gene expression selectively prolongs survival of growth factor-deprived hemopoietic cell lines. *J Immunol* 144:3602–3610.
24. Saraste A, Pulkki K (2000) Morphologic and biochemical hallmarks of apoptosis *Cardiovasc Res* 45:528–537.
25. Mangi MH, Newland AC (1999) Interleukin-3 in hematology and oncology: Current state of knowledge and future directions. *Cytokines Cell Mol Ther* 5:87–95.
26. Korpelainen EI, Gamble JR, Vadas MA, Lopez AF (1996) IL-3 receptor expression, regulation and function in cells of the vasculature. *Immunol Cell Biol* 74:1–7.
27. Mantovani A, Allavena P, Sica A, Balkwill F (2008) Cancer-related inflammation. *Nature* 454:436–444.
28. Ishii KJ, Akira S (2006) Innate immune recognition of, and regulation by. *DNA Trends Immunol* 27:525–532.
29. Morgenstern JP, Land H (1990) Advanced mammalian gene transfer: High titre retroviral vectors with multiple drug selection markers and a complementary helper-free packaging cell line. *Nucleic Acids Res* 18:3587–3596.